JAAS

Accepted Manuscript

This is an *Accepted Manuscript*, which has been through the Royal Society of Chemistry peer review process and has been accepted for publication.

Accepted Manuscripts are published online shortly after acceptance, before technical editing, formatting and proof reading. Using this free service, authors can make their results available to the community, in citable form, before we publish the edited article. We will replace this *Accepted Manuscript* with the edited and formatted *Advance Article* as soon as it is available.

You can find more information about *Accepted Manuscripts* in the Information for Authors.

Please note that technical editing may introduce minor changes to the text and/or graphics, which may alter content. The journal's standard Terms & Conditions and the Ethical guidelines still apply. In no event shall the Royal Society of Chemistry be held responsible for any errors or omissions in this *Accepted Manuscript* or any consequences arising from the use of any information it contains.

ROYAL SOCIETY OF CHEMISTRY

www.rsc.org/jaas

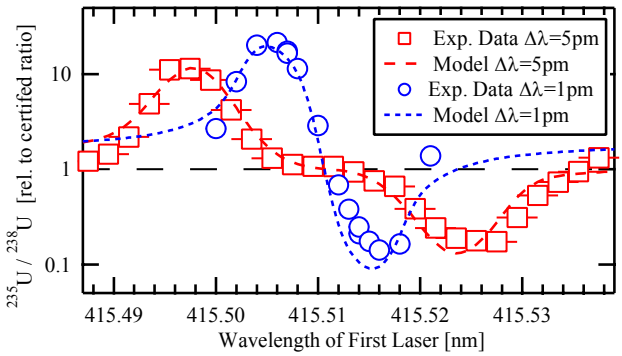

RIMS rate equation model of uranium ionization to facilitate the study of laser induced bias on measured isotope ratios

Rate Equation Model of Laser Induced Bias in Uranium Isotope Ratios Measured by Resonance Ionization Mass Spectrometry

B.H. Isselhardt[1], S.G. Prussin[2], M.R. Savina[3], D.G. Willingham[4], K.B. Knight[1], I.D. Hutcheon[1]

(1) Lawrence Livermore National Laboratory, (2) University of California at Berkeley, (3) Argonne National Laboratory, and (4) Pacific Northwest National Laboratory

Abstract

Resonance Ionization Mass Spectrometry (RIMS) has been developed as a method to measure uranium isotope abundances. In this approach, RIMS is used as an element-selective ionization process between uranium atoms and potential isobars without the aid of chemical purification and separation. The use of broad bandwidth lasers with automated feedback control of wavelength was applied to the measurement of the $^{235}U/^{238}U$ ratio to decrease laser-induced isotopic fractionation. In application, isotope standards are used to identify and correct bias in measured isotope ratios, but understanding laser-induced bias from first-principles can improve the precision and accuracy of experimental measurements. A rate equation model for predicting the relative ionization probability has been developed to study the effect of variations in laser parameters on the measured isotope ratio. The model uses atomic data and empirical descriptions of laser performance to estimate the laser-induced bias expected in experimental measurements of the $^{235}U/^{238}U$ ratio. Empirical corrections are also included to account for ionization processes that are difficult to calculate from first principles with the available atomic data. Development of this model has highlighted several important considerations for properly interpreting experimental results.

Preprint submitted to JAAS *November 20, 2015*

Introduction

Accurate uranium isotope ratio measurements are critical quantities in the examination of nuclear materials for environmental, non-proliferation, forensic, and safeguards purposes [1]. Traditional mass spectrometric methods, such as inductively coupled plasma mass spectrometry, thermal ionization mass spectrometry, or secondary ionization mass spectrometry, for quantifying these ratios rely on chemical purification or high mass resolution to eliminate or reduce isobaric interferences [1, 2]. In contrast, resonance ionization mass spectrometry (RIMS) takes advantage of the unique atomic structure of individual elements, using laser beams to ionize neutral atoms of a particular element, where the wavelengths of the laser beams are selected to excite specific electronic transitions. This approach not only provides the capability to determine the mass-to-charge ratio of ions using mass spectrometric methods, but also the opportunity to distinguish the atomic number of resonantly ionized atoms during the ionization process. To date, the application of RIMS has largely been limited to environmental studies and the analysis of extra-terrestrial samples [3–9] due to challenges in laser performance and reliability, as well as differences in the relative ionization probability between isotopes of a given element.

Recent advancements in the application of RIMS to quantify uranium isotope ratios in nuclear materials have demonstrated the use of broad bandwidth (~10 GHz) laser beams to mitigate the influence of the isotope shift between atomic levels in ^{235}U and ^{238}U [10–13]. While not completely eliminating the influence of laser-induced isotope fractionation during ionization, this approach decreases the requirements of laser system performance necessary for reproducible measurement of uranium isotope abundances. The required laser beam spectral distributions and irradiance are achievable practically, allowing uranium and plutonium isotope ratios of unknown materials to be quantified by comparison with standards to account for isotopic fractionation in the measurement

system [12, 14]. Successfully applying this approach requires demonstrating the reproducibility of laser-induced fractionation over the time periods required to measure both standards and unknowns.

We have developed a rate-equation model for calculating the relative ionization probability of ^{234}U, ^{235}U, and ^{238}U under the conditions of resonance ionization used in our work [10–13, 15] in order to predict the influence of variations in laser beam parameters on the measured $^{234}U/^{238}U$ and $^{235}U/^{238}U$ isotope ratios, and thus, to better understand and quantify the sources of laser-induced fractionation. There are two potential types of isotopic fractionation in RIMS. The first is the mass-dependent fractionation that occurs in essentially all mass spectrometers due to differential production, transmission, or detection of ions based on their mass-to-charge ratio [16]. The second, unique to laser ionization methods, is a mass-independent fractionation induced by the spectroscopic differences between isotopes of a given element. Small differences in the energy of electronic excited states between different isotopes within an element (~1 part in 10^5 for U), referred to as the isotope shift, and the influence of hyperfine structure (HFS) [17, 18] determine the variation in response of different isotopes under laser irradiation.

The systematics of isotope ratio measurements with resonant laser photoionization sources have been outlined by Wunderlich, *et al.* [19, 20], who divided laser-induced fractionation into three effects: (I) wavelength tuning and bandwidth effects, (II) dynamic effects, and (III) selection rules and polarization effects. The superposition of the laser beam spectral irradiance with the atomic resonances (I) will determine which isotopes are resonantly excited from one state to another; differences in energy for the resonant transitions of various isotopes can lead to differences in the probability of excitation for each isotope, depending on the mean wavelength and bandwidth of the laser beam. Even with comparable overlap of the laser beam spectral distribution

with the atomic resonance energies, differences in the ionization probabilities can arise from the HFS of isotopes with non-zero nuclear spin. The HFS arises from the coupling of nuclear and electronic angular momentum, which increases the number of available excited states, lifting the degeneracy of magnetic substates and influencing transition probabilities. Dynamic effects (II) were explored theoretically by Lambropoulos and Lyras [21, 22] for a simple system, the naturally occurring isotopes of Sn, where the total angular momentum is restricted to values of 0, 1/2, 1, and 3/2; they demonstrated that the odd-A and even-A isotopes of Sn do not ionize equally, due to different rates of redistribution of populations between states and rates of ionization. Finally, the restrictions on allowed dipole transitions based on angular momentum effects under certain polarization conditions (III) can cause large variations in the transition probabilities [23] and can even cause population trapping [24, 25]. The effects of selection rules on ionization probability are easily mitigated by intelligent selection of the ionization scheme (*i.e.*, transitions with $\triangle J = +1$) to ensure that an equal ratio of degenerate substates are accessible for even-A and odd-A isotopes. These studies and others demonstrate that judicious choices of laser beam parameters and excitation schemes can minimize the influence of isotope-dependent ionization probability differences, but are often insufficient to provide equal ionization probability for two isotopes. With a more extensive theoretical study of the ionization scheme and laser beam parameters it should be possible to anticipate the effects on isotope ratio measurements for all three sources of laser-induced fractionation [17, 20, 21]. This was the main motivation for developing a model of relative ionization probability for uranium isotopes.

Substantial work exists in the literature with regard to relative ionization probability of simple two- and three-state systems using the density matrix approach (or Bloch equations) [17, 18, 21, 26–28]. On the other hand, the density matrix treatment for complicated systems, such as

uranium, has not been conducted as a result of the very large number of states and transitions involved. Sankari, *et al*. [26] used the density matrix treatment to calculate the ionization probability for several Pu isotopes, but did not include any odd-A isotopes. The significance of understanding the details of the photo-ionization of ^{235}U and its large total angular momentum ($F_{max} = 19/2$ in the ground state) led to the use of rate equations in the present work. The limits of accuracy of the rate equations under conditions of coherent excitation are known, and in general, for incoherent excitation over a large number of samplings, the results of rate equation and density matrix predictions agree well[1]. For predictions far away from the resonance centroid, where contributions to the cross sections are no longer dominated by single isolated resonances, the rate equation model is expected to fail [27], however, this is not expected to be significant for our model.

We present herein a rate equation model for predicting the relative ionization probabilities of uranium isotopes to study the effect of variations in laser parameters on the measured ^{235}U/^{238}U isotope ratios. The model has been developed to highlight the most significant factors affecting the relative ionization probabilities of ^{235}U and ^{238}U, and the sensitivity of measured isotope ratios to these factors. After a brief introduction to the resonance ionization scheme, the model and its assumptions are presented, followed by a description of the method for calculating cross sections for both even and odd isotopes. Then the experimental arrangement is described, including details of the instrument and an empirical description of the laser beams. We then use the model to estimate important constants not available in the literature, such as ionization cross sections, fixing their values by comparison to measured data. Finally, we present a comparison of the model with the measured ^{235}U/^{238}U ratio as a function of wavelength for several experiments, demonstrating the

[1]We expect incoherent interactions to dominate under our experiment conditions of reasonably broad bandwidth excitation and with irradiances that vary slowly on time on the scale of the Rabi oscillations.

ability of the model to predict the sensitivity of the measurements as a function of laser irradiance and bandwidth.

Resonance Ionization Scheme for ^{235}U and ^{238}U

We employed the 3-photon, 3-color ionization scheme from Schumann *et al.* [29]. Figure 0.1 shows a partial energy level diagram of uranium showing the ionization scheme for ^{235}U and ^{238}U including the energy and angular momentum of the levels involved and the wavelengths of the laser beams used to excite each transition. The scheme excites uranium atoms from their ground level ($E = 0\,\mathrm{cm}^{-1}, J = 6$) to the first excited level[2], which has odd parity, a total angular momentum of $J = 7$, and an energy of 24,066 cm^{-1}. The second transition excites the atoms from the first excited level to a level near 36,128 cm^{-1} with $J = 8$. Finally, the excited atoms are ionized by excitation to a very broad (30 GHz) autoionizing state at 49,974.544 cm^{-1} with $J = 8$. Compared to the isotopically selective application of the ionization scheme by Schumann *et al.* [29], we were interested in achieving approximately equal ionization probabilities for several isotopes and so use wavelengths centered between the wavelengths corresponding to the centroids of ^{235}U and ^{238}U resonances for each transition. Therefore, the mean wavelengths used to excite the above transitions are $\lambda_1 = 415.5105$ nm, $\lambda_2 = 829.089$ nm, and $\lambda_3 = 722.200$ nm with sufficient laser bandwidth to excite both isotopes simultaneously.

^{235}U has a ground-state spin of $7/2$ and its level structure is quite complicated in comparison to those of the even-A uranium isotopes. Schumann *et al.* [29] measured the hyperfine structure of ^{235}U, and this facilitates the calculation of the energy of individual transitions using the Casimir

[2]The electron configuration for this level is $5f_3 6d 7s_2 7p$, with a level term assignment of ^{5}L. The other excited states do not have known electron configurations or term level assignments, only angular momentum and parity are known.

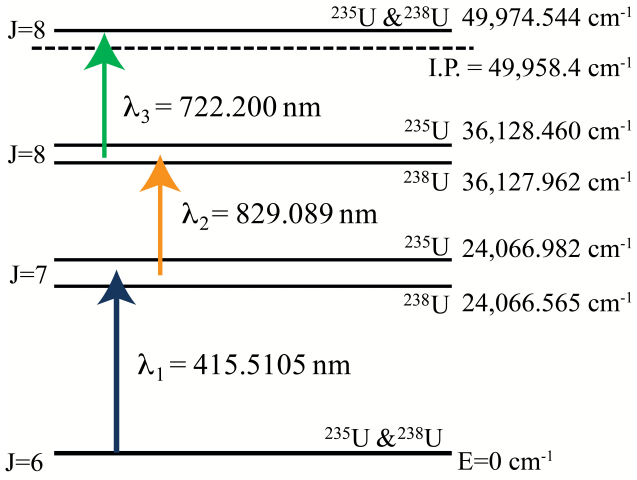

Figure 0.1: A 3-color, 3-photon U ionization scheme. This partial energy diagram shows the isotope shift between the levels of ^{235}U and ^{238}U used in this scheme and the wavelengths of the lasers used to excite the transitions between these levels. On the left are the total electron angular momenta of the levels.

formula [29, 30]. Table 1 lists the values of the mean ^{235}U isotope shift relative to each level of ^{238}U and the measured constants A and B reported in Schumann *et al.* and Childs *et al.* [29, 30]. The A and B constants have not been determined for the autoionizing resonance at 49,974.544 cm^{-1}.

Table 1: Isotope shifts and hyperfine constants in ^{235}U [29, 30]. The isotope shift in ^{235}U is reported as the mean energy of the hyperfine states relative to ^{238}U. The A and B constants are used to define the energy of individual hyperfine states of ^{235}U. Errors are given as 2σ.

Energy of ^{238}U level [cm^{-1}]	^{235}U Isotope Shift [MHz]	A [MHz]	B [MHz]
0	0	-60.559(3)	4,104.15(20)
24,066.565	12,511.97(58)	-108.172(35)	2,074.44(28)
36,127.962	14,913.80(44)	-105.639(24)	3,269.7(23)
49,974.544	unknown	unknown	unknown

Model of Relative Ionization Probability

The model is intended to represent the relative ionization probabilities of uranium isotopes from their atomic ground state via the 3-step ionization pathway described above. During model development it became clear that additional ionization pathways had to be included in order to more closely represent experimental measurements. These include non-resonant background signals at m/z corresponding to atomic uranium ions, as well as an alternative 3-step process using photons from only two of the three lasers. The data required for calculating ionization cross sections are not found in the literature, and thus, were estimated by fitting the model predictions to experiment data. The methods for accomplishing this are described in Section 4.

The model uses calculations of an average cross section for each transition to describe the behavior of an ensemble of atoms under the influence of laser photons. In the limit that we are interested only in the average result over a large number of samples, the average cross section should be a good description of the quantum mechanical probabilities. In the experiments, each measurement consists of $10^4 - 10^5$ individual laser and atom pulses.

In the experiments, the ionization of atoms occurs in a volume defined by the overlap of the photon beams with the spatial distribution of sputtered neutral atoms and molecules. The complexity of this spatial dependence, and the fact that the measured isotope ratios represent an average over these spatial distributions, is not accurately represented in our model. Rather, we choose to use a simplified, dimensionless model of the average photon flux interacting with an ensemble of atoms. As a result we cannot accurately account for the difference between the laser power as measured during experiments and the average laser irradiance consistent with the simplifications of the model. It is reasonable, however, to assume a linear relationship in irradiance for experiments that

used laser beams with nearly the same spatial distributions[3].

Rate Equations

The model calculates the population density of four specific states of a uranium atom as the atoms are irradiated by the excitation lasers: the ground level, two bound excited levels, and an ionizing level. The four equations describing the rate of change of the populations of each level are

$$\frac{dN_0}{dt} = W_{01}(N_1 - \frac{g_1}{g_0}N_0) + \frac{N_1}{\tau_1} \quad (0.1)$$

$$\frac{dN_1}{dt} = W_{01}(\frac{g_1}{g_0}N_0 - N_1) + W_{12}(N_2 - \frac{g_2}{g_1}N_1) - \frac{N_1}{\tau_1} + \frac{N_2}{\tau_2} \quad (0.2)$$

$$\frac{dN_2}{dt} = W_{12}(\frac{g_2}{g_1}N_1 - N_2) - \frac{N_2}{\tau_2} - W_{2ion}N_2 - W_{2C}N_2 \quad (0.3)$$

$$\frac{dN_{ion}}{dt} = W_{2ion}N_2 + W_{2C}N_2 \quad (0.4)$$

where N_i is the number of atoms in state $|i\rangle$, W_{ij} is the rate of the transition per atom from state $|i\rangle$ to state $|j\rangle$, g_i is the degeneracy factor ($g_i = g_j$ for linearly polarized light) for state $|i\rangle$, and τ_i is the average lifetime of state $|i\rangle$. We have assumed that all spontaneous decay occurs to states within the scheme, and that the probabilities for collisional relaxation and radiative decay to states outside the level scheme are small relative to the probabilities for laser excitation and can be ignored[4]. Decay from the $|ion\rangle$ state back to the bound states is neglected, as the probability for autoionizing states

[3]We expect that this approximation is acceptable for resonance processes that are linearly proportional to photon flux, as long as the atoms are not concentrated in a volume not well described by the average photon flux. For non-resonant processes that are non-linear with respect to the photon flux, this approximation is inappropriate. We assume that photon attenuation can safely be neglected and that the cross-sectional area of the laser beam is constant within the ionization volume. These assumptions reduce the consideration of the photon flux to the cross-sectional area of the laser beam, assumed to have a 2-D Gaussian intensity profile.

[4]Note that state$|2\rangle$ cannot decay back to the ground state via a single photon emission due to parity conservation.

to decay by electron emission is often six orders of magnitude larger than for photon emission. In order to consider additional ionization pathways, terms of the form $\pm W_{2C}N_i$ are added to express the rate of ionization into the continuum (C) from state $|2\rangle$, where the negative term is added to the equation for state $|2\rangle$ and the positive term is added to the equation for the $|ion\rangle$ state. Within the limits of numerical integration, approximate solutions to equations $0.1-0.4$ can be calculated once the rates W_{ij} have been defined. We assume that all atoms are initially in the ground state, and the equations are numerically integrated as a function of time for a period long compared to the laser pulse widths. After the integration, the cumulative fraction of ions produced is recorded.

The transition rates are defined as the spectral overlap of the time-dependent spectral irradiances of the lasers with the cross sections of the atomic states and are given by

$$W_{ij} = \int\int \sigma_{ij}(\lambda)\cdot I_i(\lambda,t)\,\mathrm{d}\lambda\,\mathrm{d}t \cong \sum_{m=0}^{l}\sum_{k}\sigma_{ij}(\bar{\lambda}_k)\cdot I_i(\bar{\lambda}_k, m\cdot\Delta t)\,\Delta\lambda\,\Delta t \qquad (0.5)$$

where $\sigma_{ij}(\lambda)$ is the cross section for the transition between state $|i\rangle$ and state $|j\rangle$ expressed as a function of wavelength, and $I_i(\lambda,t)$ is the spectral irradiance of the laser used to excite that transition (the lasers are numbered using the excitation order of our ionization scheme). In the model, the integrals are replaced by a summation over finite elements of width $\Delta\lambda$ extending over the wavelength range of the irradiance. The summation over time is the sum over l time intervals of Δt. The superscript bars represent evaluation of the quantity at the average wavelength of each discrete element.

The transition rate is a function of the time-varying amplitude of the laser pulses, but because the time dependence is largely independent of wavelength, the time dependence is treated as an

independent function. The transition rate is then expressed by

$$W_{ij}(t) = W_{ij} \cdot T_i(t) \tag{0.6}$$

where $T_i(t)$ is the time distribution of a pulse produced by the laser used to excite the transition. In the model, the pulse shape is assumed to be Gaussian and given by

$$T_i(t) = \frac{1}{\sqrt{2\pi\sigma^2}} \mathrm{e}^{-\frac{(t-T_0)^2}{2\sigma^2}}$$

where σ is the standard deviation and T_0 is the time corresponding to the peak intensity. The FWHM of the laser pulses were measured to be 14 ± 4 ns in the fundamental wavelength range or 26 ± 6 ns for the 2^{nd} harmonic wavelengths, where the quoted uncertainties represent twice the standard deviation of the pulse-width measurements. The differences in pulse width are the result of differences in the laser beams used to pump the respective cavities. In practice, pulses from the three Ti:Sapphire cavities are produced with some distribution in time. On average, the observed distribution of T_0 for relative timing between the three lasers in the experiments can be approximated as a normal distribution with a FWHM of ~ 4 ns.

Cross Sections

The cross section for absorption as a function of wavelength from a given substate m_i of state J_i for a level $|i\rangle$ to a substate m_j of state J_j for a level $|j\rangle$ in an atom is expressed as

$$\sigma_{m_i m_j}(\lambda) = \frac{\lambda_0^2 \cdot \Gamma_{ji}}{4} k(\lambda) = \frac{2\pi^2 k(\lambda)}{3\varepsilon_0 \hbar \lambda_0} |D_{ij}|^2 \tag{0.7}$$

where λ_0 is the mean transition wavelength, Γ_{ji} is the partial width of the excited state[5], $k(\lambda)$ is the normalized lineshape of the transition, ε_0 is the permittivity of free space, and $|D_{ij}|^2$ is the squared magnitude of the dipole matrix element for the transition. Note that the degeneracy factor g_j/g_i is not included when dealing with specific substates.

Calculating Transition Cross Sections for Even Isotopes. The cross section as a function of wavelength is calculated as the product of the amplitude at the wavelength corresponding to the peak cross section and a normalized lineshape

$$\sigma_{ij}(\lambda) = \sigma_0 \cdot k(\lambda) \tag{0.8}$$

where $\sigma_0 = \frac{\lambda_0^2}{4}\Gamma_{ji}$ is the peak cross section and $k(\lambda)$ is given by the lineshape profile of the transition. The lineshape is dependent on the natural linewidth of the transition and the velocity distribution of the atoms in the ionization volume. Atoms will have a velocity distribution based on the sputtering or desorption process used for atomization. We assume that the velocity distribution of atoms in the gas phase follows a Maxwell-Boltzmann distribution, resulting in Doppler broadening of the natural lineshape. The actual lineshape is then a convolution of a Gaussian function with a Lorentzian function.

The cross section for transitions in even isotopes is then of the form

$$\sigma_{even}(\lambda) = \frac{\lambda_0^2}{4}\Gamma_{ji} \cdot \frac{g_j}{g_i} \cdot [\mathscr{D}(\lambda) \otimes \mathscr{L}(\lambda)] \tag{0.9}$$

where $\mathscr{D}(\lambda)$ is the Doppler broadened lineshape and $\mathscr{L}(\lambda)$ is a Lorentzian function describing the

[5] We assume that $\Gamma_{ij} = \Gamma_{ji}$ and that the width of the initial state does not contribute significantly to the cross section.

natural linewidth of the resonance.

Influence of Nuclear Spin

The cross sections of odd isotopes must account for the small differences in resonance wavelength of each of the transitions between magnetic substates and properly distribute the transition probabilities across these individual transitions. The ionization scheme of central interest here involves exciting ground state atoms of uranium ($J_{|0\rangle} = 6$) to an excited level at 24,066 cm^{-1} with $J_{|1\rangle} = 7$. The coupling of atomic to the nuclear spin in ^{235}U ($I = 7/2$) leads to eight possible non-degenerate states of total angular momentum $F_{|0\rangle} = [19/2, 17/2, ...5/2]$and $F_{|1\rangle} = [21/2, 19/2, ...7/2]$. In addition, each of these levels is composed of $2F + 1$ magnetic substates, m_F (which are degenerate in the absence of an external electromagnetic field). This leads to 104 total substates in the ground level and 120 total substates in the first excited level.

Figure 0.2 is an atomic energy level diagram of ^{235}U showing the eight non-degenerate angular momentum states created by the coupling of the nuclear spin to either the ground or first-excited atomic levels in our resonance ionization scheme. The individual F states are shown along with their energy in MHz relative to the average energy of the level, and are calculated by the Casimir formula with the A & B values from Schumann *et al.* [29]. There are 21 unique transition energies allowed by the selection rules for linearly polarized light ($\triangle F = 0, \pm 1$, where if $\Delta F = 0$, $m_i = m_j = 0$ transitions are forbidden). Each unique transition energy will have a different number of substates (m_F) allowed to participate depending on the degeneracy of the levels involved, and each transition will have a probability proportional to the square of its Clebsch-Gordan coefficient [31, 32]. Fig. 0.2 shows the transitions from the $F = 13/2$ state in the ground level to the $F = 15/2$, $13/2$ and $11/2$ states in the first excited level as examples of the set of possible transitions from a given state. Based on the selection rules for linearly polarized light, as used in our experiments,

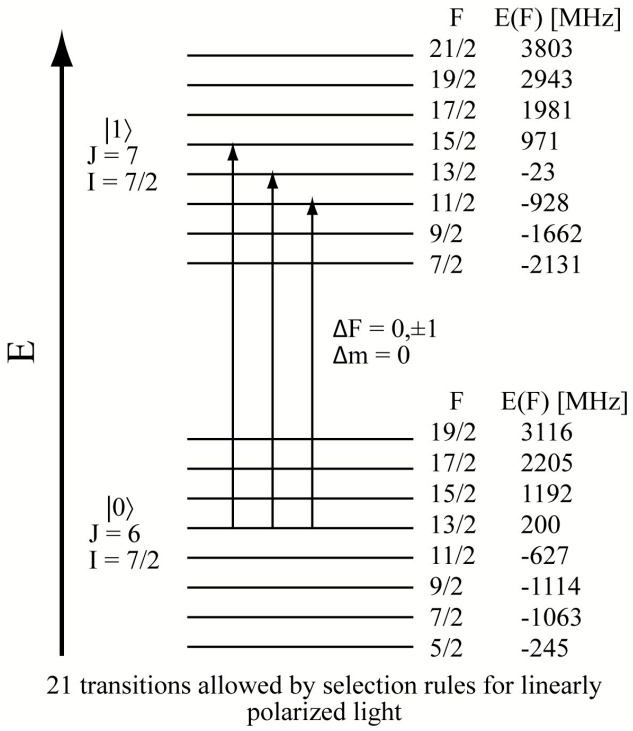

Figure 0.2: A level diagram of the first transition used in the resonant ionization of ^{235}U. The diagram shows the energy of each F state relative to the average of the eight states within each level. The arrows show three of the transitions allowed by the selection rules for dipole transitions. Each F state will have $2(F+1)$ degenerate substates.

the 14 m_F substates in the $f = 13/2$ ground state would populate only 14 of the 16 m_F substates of the $F = 15/2$ state, all 14 substates of the $F = 13/2$ state, and all 12 substates of the $F = 11/2$ state.

The Wigner-Eckart Theorem. The Wigner-Eckart theorem states that we can express the transition dipole matrix element between specific magnetic substates as the product of a reduced matrix element and the Clebsch-Gordan coefficient for the transition,

$$\left\langle J_j, m_j \left| D_{even} \right| J_i, m_i \right\rangle = C\left(J_i, J_j, \triangle J, m_i, m_j, \triangle m\right) \left\langle J_j \left\| D_{even} \right\| J_i \right\rangle \tag{0.10}$$

where $C\left(J_i, J_j, \triangle J, m_i, m_j, \triangle m\right)$ is the Clebsch-Gordan coefficient for the specific transition [32]. The reduced matrix element, $\left\langle J_j \| D_{even} \| J_i \right\rangle$, does not depend on the magnetic substates involved. In general for even-A U isotopes, the squares of the Clebsch-Gordan coefficients for transitions between each substate will sum to unity and therefore, do not need to be calculated. In this case, we define a degeneracy g_i equal to the number of substates with allowed transitions; g_i has a maximum value of $2J_i + 1$, but can be reduced when considering polarized light. In the case of our ionization scheme, the final transition is $\triangle J = 0$ eliminating the $m_i = 0$ to $m_j = 0$ transition for even-A U isotopes.

For odd-A isotopes, the degeneracy of the states within a level is removed and not every transition has equal energy. To keep track of the probability for excitation to a particular substate within each level, we adapt the Wigner-Eckart theorem to consider the total atomic angular momentum F and the reduced matrix element that depends on J but not on m_J:

$$\left\langle F_j, m_j \left| D_{odd} \right| F_i, m_i \right\rangle = C\left(F_i, F_j, \triangle F, m_i, m_j, \triangle m\right) \left\langle J_j \| D_{odd} \| J_i \right\rangle \tag{0.11}$$

$$\left\langle J_j \| D_{odd} \| J_i \right\rangle = \left\langle J_j \| D_{even} \| J_i \right\rangle \tag{0.12}$$

where $\left\langle J_j \| D_{odd} \| J_i \right\rangle$ is the reduced matrix element for the odd isotope for the transition expressed by $\left\langle F_i, m_i \left| D_{odd} \right| F_j, m_j \right\rangle$.

Calculating Transition Cross Sections for Odd Isotopes. As the cross section is proportional to the square of the transition dipole matrix element (Eqn. 7), one can multiply the peak cross section by the squared Clebsch-Gordan coefficient for a particular transition between substates, $\left\langle J_j, m_j \left| D \right| J_i, m_i \right\rangle$ as,

$$\sigma_{m_i m_j}(\lambda) = \frac{\lambda_0^2}{4} \Gamma_{ji} \cdot C(F_i, m_i, F_j, m_j)^2 \cdot k(\lambda) \tag{0.13}$$

where $C(F_i, m_i, F_j, m_j)^2$ is the squared Clebsch-Gordan coefficient between two magnetic substates. The average cross section for an odd isotope is proportional to the sum of the squared Clebsch-Gordan coefficients for each transition. Differences in transition energies as a result of differences in total angular momentum F must be taken into account. Hence,

$$\sigma_{odd} \propto \sum_F D^2_{odd} = \sum_F \left[\sum_{m_F} [C(F_i, m_{Fi}, F_j, m_{Fi})^2] \cdot D^2_{even} \right] = \sum_M C_M(F_i, m_{Fi}, F_j, m_{Fj})^2 \cdot D^2_{even} \quad (0.14)$$

where M represents each transition with unique energy, each of which is composed of degenerate transitions between $2F+1$ magnetic substates. As discussed above, there are 21 transitions with unique energies in the excitation of the first resonance of ^{235}U, but a total of 104 transitions allowed by the selection rules for linearly polarized light.

An average cross section for the allowed transitions between two levels in an odd isotope is calculated as the sum of the cross sections for each transition with unique energy convolved with the Doppler-broadened lineshape

$$\sigma_{odd}(\lambda) = \frac{\lambda_0^2}{4} \Gamma_{ji} \cdot \frac{1}{(2J+1)(2I+1)} \left[\mathscr{D}(\lambda) \otimes \sum_M \left(C_M(F_i, m_{Fi}, F_j, m_{Fj})^2 \cdot \mathscr{L}_M(\lambda) \right) \right] \quad (0.15)$$

where M represents the sum of degenerate transitions between substates for a transition of unique energy and $\mathscr{L}_M(\lambda)$ represents the Lorentzian lineshape of the transition. Unlike transitions in even-A isotopes, the quantity in square brackets is no longer normalized to unity because of the squared Clebsch-Gordan coefficients. The lineshape is normalized by the total statistical weight of the initial level, $(2J+1)(2I+1)$, to account for the increased number of states [33]. For the first transition in ^{235}U the sum of the squared Clebsch-Gordan coefficients is 98.67, while the statistical weight of the ground level is 104.

Table 2: Atomic parameters for ^{235}U and ^{238}U used in the model [29, 35–39]. Errors are given as 2σ.

Resonance ^{238}U [nm]	Resonance ^{235}U [nm]	Lifetime or Width	Doppler Estimate [pm]
415.514	415.5068	57(6) ns	2.05
829.091	829.087	215(20) ns	4.08
722.202	722.200	52(2) pm	3.57

A summary of the parameters used to calculate the atomic cross sections is found in Table 2, which gives the wavelengths of the resonance transitions used in ^{235}U and ^{238}U, the lifetime or width of the excited states, and an estimate of the Doppler broadening in wavelength. The resonance transition to the autoionizing state of 722.200 nm for ^{235}U is an estimate, but the isotope shift is small compared to the 0.052 nm width of the resonance. Our initial estimate of the Doppler broadening, based on a general rule of thumb for ion sputtering, assumes a Maxwell-Boltzmann distribution of 1 eV, about 3 times the melting temperature of UO_2. Typical energies of sputtered U atoms are between $2-5$ eV, but are strongly forward directed Wright *et al.* [34]. Doppler broadening in our experiments is caused by velocity components of atoms that are parallel to the laser beams (orthogonal to the ion flight trajectory through the mass spectrometer), thus observed Doppler widths are best described using a lower temperature estimate of 1 eV.

The challenge for performing analytical measurements, posed by the presence of large isotope shifts, is clearly exemplified in the electric dipole transition for atomic uranium for the first transition in our scheme. Figure 0.3 shows the calculated cross sections of this resonance transition for ^{235}U and ^{238}U as a function of wavelength. The cross section for ^{235}U on the left side of the figure is centered at 415.507 nm and the cross section for ^{238}U on the right is centered at 415.514 nm. The peak for ^{238}U is approximately 3.5 GHz wide (FWHM), including both the natural width of

the resonance (~2.8 MHz) and the estimated Doppler broadening of the transition (~3.5 GHz). The peak for ^{235}U is larger and broader due to the inclusion of the hyperfine splitting discussed above. The mean wavelengths of the resonances are separated by approximately 12.5 GHz. Also shown in Fig. 0.3 are two Gaussian models for the laser spectral distribution (dashed lines). The 1 pm (1.7 GHz) laser model represents the nominal spectral distribution produced by our laser system at this wavelength. The 5 pm (8.7 GHz) laser model represents a broadened spectral distribution, which provides significantly improved overlap of both resonances. The broad distribution can sufficiently excite this transition in both isotopes simultaneously at practical intensities while the narrow distribution cannot. Additionally, with the broad distribution, the excitation probability for both isotopes will be less dependent on pulse-to-pulse variations in mean wavelength Isselhardt *et al.* [11].

Instrument and Experiment Descriptions

Description of Instrument. The instrument used was the Chicago-Argonne Resonance Ionization Spectrometer for Microbeam Analysis (CHARISMA) [7, 40]. It consists of a primary ion gun for sputtering (or, optionally, a laser desorption system), a solid state tunable laser ionization system, ion extraction and focusing optics, a reflectron time-of-flight (TOF) mass analyzer, and a fast data acquisition system. Analysis with CHARISMA proceeds as follows: (1) a pulse of energetic Ga^+ ions impacts the surface of a target producing a cloud of neutral atoms, ions and molecules; (2) a voltage pulse is applied to the target to electrostatically separate ions from neutrals in the cloud; (3) photons from two or more Ti:sapphire lasers intersect the cloud of neutral species above the sample, resonantly ionizing atoms of the element of interest with close to 100 % efficiency; (4) a high voltage pulse extracts and accelerates the photo-ions into the TOF mass spectrometer for analysis. Generally, the combination of high ionization efficiency and high elemental selectivity

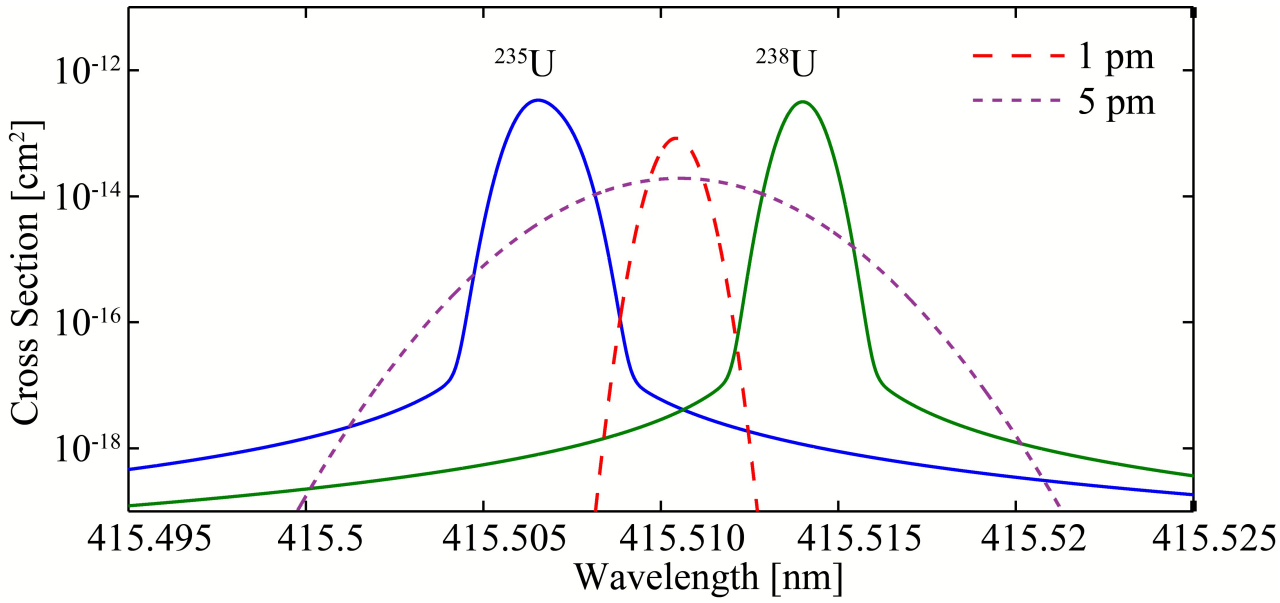

Figure 0.3: Cross sections for ^{235}U and ^{238}U as a function of wavelength for the first resonance transition in our scheme (Fig. 0.1). The ^{238}U resonance is approximately 3.5 GHz wide (FWHM) and the peaks are separated by about 12.5 GHz. Superimposed on these resonances are two Gaussian models for the spectral distribution of the resonance laser with FWHM of 1 and 5 pm (1.7 GHz and 8.7 GHz), both of the same total intensity. The amplitudes of the laser models are arbitrary relative to the resonance cross sections.

gives an overall detection efficiency (ratio of ions detected to atoms removed by sputtering for a given species) of $> 2.5\,\%$, although for uranium this number is typically much lower due to the sputtering of uranium oxide molecules. The experiments performed for this work have been described in Isselhardt *et al*., and Willingham *et al.* [11, 15].

The instrumental mass-dependent isotope fractionation is assumed to be negligible compared to laser effects. Measurements have demonstrated that the $^{235}\mathrm{UO}/^{238}\mathrm{UO}$ ratio (non-resonantly ionized molecules) deviates from the certified ratio by less than $0.3\,\%$. In addition, any bias due to instrumental effects would be constant across the variations in model parameters, and corrections for this effect could be applied after the model computations.

Description of Lasers. The laser system is composed of three nearly identical Ti:sapphire cavities each pumped by a Nd:YLF laser. Each Ti:sapphire cavity is tunable over the wavelength range $700 - 1000\,\mathrm{nm}$ via a gold-coated grating that functions as an end mirror. The cavities use a simple box design with two turning mirrors, a Ti:sapphire crystal, an output coupler, a beam expander, and a reflective diffraction grating. The grating is secured on a rotational mount that turns in the horizontal plane of the cavity. The second-harmonic (2ω) of the Ti:sapphire fundamental beam is produced in a LBO crystal located just outside of the cavity. Each laser beam is then collimated and shaped separately before entering the target chamber using cylindrical lenses.

The tunable cavities nominally produce laser beams with bandwidths in the fundamental range of $1.3\,\mathrm{GHz}$[6]. We employed beam expanders with different magnification factors to illuminate more or fewer lines on the diffraction grating and thus create laser beams with varying bandwidths. A 4X expander produced the smallest magnification with which we were able to obtain stable laser

[6] 1.3 GHz is 3 pm at 830 nm and 2.2 pm at 722 nm. When a beam from this arrangement is frequency-doubled into the 415 nm range the result is a bandwidth of 1.8 GHz or about 1 pm.

oscillation in the cavities and generated a laser bandwidth of 6 – 10 GHz. When frequency doubled, the bandwidth of this arrangement was in the range 9 – 13 GHz or about 5 pm.

Laser Spectral Irradiance. The time-independent spectral irradiance $I_i(\lambda)$ of each laser beam is the product of the photon flux (ϕ_i) and a normalized spectral distribution ($l(\lambda)$), and can be written as

$$I_i(\lambda) = \phi_i \cdot l(\lambda)$$

The photon flux of laser beam i is given by Hurst [41] as

$$\phi_i[\text{photons}\cdot\text{cm}^{-2}] = \left(5 \cdot 10^9\right) \cdot (\lambda_i[\text{nm}]) \cdot (P_i[\mu\text{J}])\,/A[\text{cm}^2] \tag{0.16}$$

The wavelength (λ), pulse intensity (P_i), and area (A) of the laser beams are experimental variables that can be explored within the model. In practice, lasers exhibit fluctuations in mean wavelength, power, position, and timing from pulse to pulse. These fluctuations are the main limitation in the precision of isotope ratios measured by RIMS. To reproduce the effects of pulse-to-pulse wavelength fluctuations over a large number of pulses, the model calculates a distribution of ionization probabilities across the wavelength range of interest and then, for each mean wavelength value chosen, randomly samples this distribution 100,000 times using a normal distribution with a standard deviation set to the specified wavelength fluctuation. This approach of calculating ionization probabilities for discrete laser wavelengths, representing individual laser pulses, and then averaging the results based on the variation expected during experiments provides a greatly improved in contrast to the results reported in [10]. Table 3 gives the range of laser wavelengths, laser pulse energies, and bandwidths studied and also includes the measured values for the pulse-to-pulse fluctuations

Table 3: Range of laser parameters explored in the model.

Laser No.	Wavelength [nm]	Pulse Energy [μJ]	Bandwidth [pm]	Wavelength Fluctuation [pm]	Time Fluctuation [ns]
1	415.48−415.54	0−600	1−10	2−8	4−14
2	829.08−829.10	0−1000	3	3	4−14
3	722.200	0−700	3	3	4−14

Table 4: Standard materials and their certified isotope abundances in atomic percent. Errors are reported as 95 % confidence intervals as reported on certificates [42, 43].

Material	Composition	U Content [wt %]	^{238}U[at %]	^{235}U [at. %]
CRM 112-A	U metal	100(5)	99.27458(39)	0.72017(39)
U500	U_3O_8	84.7(1)	49.711(50)	49.696(50)

in wavelength and pulse timing of the lasers.

Description of Standards. CRM 112-A (available from New Brunswick Laboratory, formerly known as SRM 960) is a U metal standard of natural isotopic composition with a uranium oxide surface layer from prolonged exposure to air. The standard was mounted on an aluminum stub 1.27 cm in diameter with conductive epoxy. We also used CRM U500 (also available from New Brunswick Laboratory), highly purified U_3O_8 enriched to approximately 50% in ^{235}U. This standard was mounted by pressing the grains of material into an indium metal foil which in turn was pressed onto the aluminum stub. Both standards are certified for their isotope abundances of ^{235}U and ^{238}U, as given in Table 4 along with their stated uncertainties [42, 43]. Each sample contained approximately ~100 μg of each standard, only a small fraction of this mass was used for analysis and the analytical spots were sufficiently small to sputter only the uranium materials.

Model Results

In order to compare the relative ionization probabilities obtained from the rate equation model with experiments, we must consider all processes that contribute significantly to the measured ion signals. At least two ion formation processes under resonant ionization conditions were observed, ionization through the autoionizing state and a 2-color, 3-photon ionization pathway, in which a photon from the first laser (415 nm) promotes an electron from the second excited state into the ionization continuum. The cross sections for these two processes cannot be calculated from data available in the literature, and must instead be estimated by examining the dependence of the ionization probability on the intensity of the laser fluence exciting the atom into an ion. In addition to these resonance pathways, under all ionization conditions there is a non-negligible production of ions by non-resonant processes that contributes to the measured ion signal.

Autoionizing Cross Section. The desired pathway for ionization is a transition from the second excited state to an autoionizing state induced by a 722.200 nm photon. The calculation of the ionization cross section requires integration of the probability of transitions to autoionizing states as well as continuum states and involves detailed angular momentum and radial descriptions of the wavefunctions that are complex for uranium. As the wavelength dependence of the first and second resonance transitions are the primary focus of this work, the autoionizing cross section is simply approximated as a discrete transition where the last photon absorbed excites the atom above the ionization limit, and then decays by ionization. This neglects ionization from excitation to the continuum from outside of the autoionizing state, but the probability for this process must be several orders of magnitude smaller than excitation into the discrete autoionizing state, and can be considered negligible.

The full width of the autoionizing state can be written as

$$\Gamma = \sum_i \Gamma_i = \Gamma_{\gamma\gamma} + \sum_{\gamma'} \Gamma_{\gamma\gamma'} + \Gamma_{e^-} \tag{0.17}$$

where the total width Γ is the sum of the partial widths of all possible decay modes (Γ_i). The widths on the right-hand side of equation 0.17 correspond to the partial width of the autoionizing state to decay back to the second excited state ($\Gamma_{\gamma\gamma}$), the sum of all other possible photon transitions ($\Gamma_{\gamma\gamma'}$), and the partial width for electron emission (Γ_{e^-}). Neglecting Doppler broadening, the peak cross section (when $E = E_0$) is written as

$$\sigma_{\gamma\gamma} = \frac{g_2}{g_1} \frac{\lambda_0^2}{2\pi} \cdot \frac{\Gamma_{\gamma\gamma}}{\Gamma} \tag{0.18}$$

where g_2/g_1 is the ratio of the level degeneracies and λ_0 is the transition wavelength.

The ion signals from an experiment where the irradiance of the third laser was varied from zero to almost 1 mJ while other laser parameters were held constant is shown in Figure 0.4, we compare this to the ionization probabilities predicted by the model using a cross section estimate of $\sigma_{\gamma\gamma} = 1.67 \times 10^{-15}$ cm^2, where we have included the isotope-specific angular momentum considerations for excitation to the discrete autoionizing state ($J = 8$) using equations 0.9 and 0.15. The influence of the HFS in the calculated cross sections for ^{235}U is critical for fitting the data with the model predictions of enhanced ^{235}U ionization probability compared to that for ^{238}U. To estimate the cross section to the autoionizing state, the model was fit simultaneously to the ion signals from both ^{235}U and ^{238}U. Our cross section estimate is reasonably consistent with the empirical estimate from Willingham, *et al.* of 2.1×10^{-15} cm^2 [15], and corresponds to a partial lifetime for decay of the autoionizing state to the second excited state of $\sim$3.8 μs. This is long compared to the average

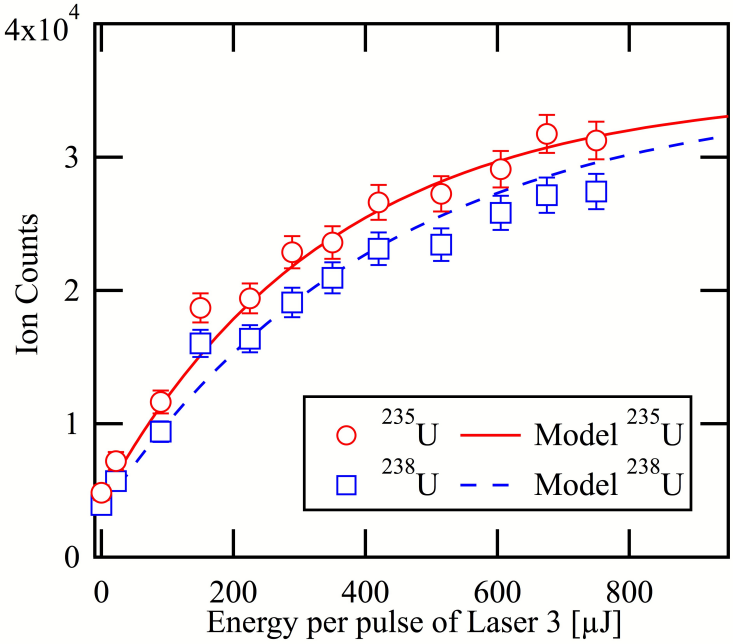

Figure 0.4: Ion signal for ^{235}U and ^{238}U as a function of the intensity of the third laser under resonance ionization conditions. The model predictions assume $\sigma_{\gamma\gamma} = 1.67 \times 10^{-15}$ cm^2, and include the angular momentum considerations for excitation to the discrete autoionizing state. Note the offset from zero arises from the 2-color, 3-photon ionization process described in the text.

total lifetime of the autoionizing state (∼5.5 ps) and the average lifetime of the second excited state (∼215 ns), and justifies neglecting decay of this state by photon emission. The ratio of the partial width to full width corresponding to this cross section is $\Gamma_{\gamma\gamma}/\Gamma = 2.08 \times 10^{-6}$.

2-Color, 3-Photon Ionization Cross Section. Experiments demonstrate a significant probability for ionizing U atoms with only photons from the first and second resonance lasers, confirming the presence of a 2-color, 3-photon ionization process. In this process, an atom is excited through the first excited state to the second excited state (36,127 cm^{-1}) by absorption of one photon each from the first and second lasers, and is then ionized by an additional photon from the first laser (415 nm, nearly 3 eV). The ion signal for this process depends linearly on the intensity of the first laser and

contributes about 10 % to the total ion signal when the energy per pulse of laser 3 is maximized. This contribution can be observed when the energy per pulse of laser 3 goes to zero, as seen in Fig. 0.4. Other, more complicated ionization pathways also exist, but require near-simultaneous absorption of at least two photons through virtual excited states. The probabilities for ionization via these pathways will be orders of magnitude smaller than for the 3-color, 3-photon pathway.

The ionization cross section for the two-color, three-photon pathway was estimated by using the model parameters for the 3-color, 3-photon on-resonance ionization conditions, but the intensity of the third laser beam was set to zero. An ionization rate (W_{2C}) was defined that represents the excitation of atoms from the second excited state into the ionization continuum due to absorption of 415 nm photons from the first laser. In the absence of an autoionizing state near the total excitation energy (60,194 cm^{-1}), this process should be essentially independent of wavelength and, thus, the rate for this transition was set equal to a constant cross section (σ_{2C}) times the integrated spectral irradiance in the first laser (I_1). The dependence of this process on the intensity of the first laser has not yet been experimentally verified, but a number of measurements across several experiments at various laser intensities provide insight into the magnitude of its cross section. Specifically, a measurement using only the first two laser beams, with 315 μJ/pulse in the first resonance beam was used. The signals for ^{235}U and ^{238}U found in this experiment were 13.0 ± 0.2 % and 12.4 ± 2 % of the maximum ion signal, respectively. Differences in the ionization probabilities through continuum states between the two isotopes are expected because of the differences in angular momentum factors of even-A and odd-A isotopes [21]; for this measurement the difference is a factor of approximately 1.05. The cross section σ_{2C} found by fitting the model to the experiment data was 7.25×10^{-17} cm^2. This is larger than the nominal theoretical cross section for absorption into the continuum of 10^{-17} cm^2 [4], but the high density of excited states in uranium may support this

larger than average cross section. This estimate was used in Fig. 0.4 for estimating the autoionizing cross section.

Non-Resonant Background. There is a small probability for producing photoions at the masses of the U^+ ions when the laser for the first transition is tuned far from resonance (off-resonance). The ion signal measured in a given mass channel under these conditions is considered to be the sum of all sources of background in the instrument (*e.g.*, non-resonant ions, dark counts, stray secondary ions, etc.). As the background can be the result of multiple complicated processes, rather than calculating the magnitude of the off-resonance signal, our model predictions are corrected empirically for specific experiments.

The off-resonance ion signal was included in the model results by first computing the ionization probability for each isotope independently, and then adding the off-resonance ion signal. The predicted $^{235}U/^{238}U$ ratio then becomes,

$$\left(^{235}U/^{238}U\right)_{predicted} = \frac{N_{ion}^{235} + N_{off}^{235}}{N_{ion}^{238} + N_{off}^{238}} \tag{0.19}$$

where the populations of the respective states represent the model predicted ionization probability (*ion*), and the off-resonance ion signal (off), and the superscripts identify the isotopes considered. This approach assumes that the off-resonance ion signal does not deplete the reservoir of available ground-state uranium atoms in the ionization volume.

The off-resonance signal was determined by comparing the detected ion signal at a given mass under two ionization conditions: on-resonance, where the wavelengths of all three laser beams were tuned to the wavelengths in Figure 0.1, and off-resonance, where conditions were the same within experimental uncertainties, except that the wavelength of the first laser beam was detuned

from the resonance condition by 0.05 nm to 415.560 nm. For experiments on CRM 112-A, when the total energy of the first laser beam was 75 μJ, the off-resonance mass 238 signal was 1.0 ± 0.1 % of the maximum on-resonance ^{238}U signal. When the energy per pulse in the first laser beam was increased to 150 μJ, the off-resonance mass 238 signal increased to 2.6 ± 0.2 % of the on-resonance ^{238}U signal. Measured differences in the off-resonance signal at mass 235 compared to mass 238 for the U500 standard show that the mass 235 signal is approximately 4.3 % of the maximum on-resonance ^{235}U ion signal. The off-resonance signal is likely dominated by photo-fragmentation and ionization of UO_X molecules in the sputtered flux. This interpretation is corroborated by the fact that the off-resonance signal is higher for measurements performed on uranium oxide solids and is greatly reduced for uranium metal targets.

It is important to quantify the actual off-resonance ion signals at both mass 235 and 238, as they have different production rates. The largest source of production of these non-resonant ions is the 415 nm photons from the laser used for the first step in the ionization scheme. The dependence of the non-resonant ion signal on the power of the first laser beam was used to develop a prediction for the magnitude of the off-resonance signal as a function of laser intensity. This provides an empirical correction to better connect our model results with measurements when appropriate off-resonance data do not exist.

Isotope Ratio as a Function of First Laser Wavelength. Two experiments were performed to study the influence of laser bandwidth on the variation in the $^{235}U/^{238}U$ ratio as a function of wavelength of the first resonance laser. The first experiment describing "narrow" laser bandwidth measurements has been reported previously [11], and involved measuring the $^{235}U/^{238}U$ ratio on CRM 112-A as a function of the wavelength of the first laser with a bandwidth of 1 pm. The wavelengths

of the second and third resonance lasers were held fixed at 829.089 and 722.344 nm[7], respectively. The total energies of the laser beams in order of excitation were 150, 900, and 540 μJ per pulse. The second experiment was performed on CRM U500 using a "broad" laser bandwidth of 5 pm, also measuring the $^{235}U/^{238}U$ ratio as a function of wavelength of the first laser. The wavelengths of the second and third resonance lasers were held fixed at 829.089 and 722.200 nm, respectively. The total energies of the laser beams in order of excitation were 75, 900, and 600 μJ per pulse.

Model calculations corresponding to these experimental conditions were performed. Using Gaussian lineshapes for the laser spectral distributions, the bandwidths of the first, second, and third lasers were fixed to agree with the relevant experiment. The wavelength of the first laser was varied from 415.480 to 415.540 nm. The second and third lasers were fixed at 829.089 and 722.200 nm, respectively. The average pulse-to-pulse variation of the mean wavelength of all three lasers was set to 2 pm for the narrow bandwidth experiment and 5 pm for the broad bandwidth experiment, as observed experimentally. The broad bandwidth experiment showed a systematic offset in the experimentally measured laser wavelengths relative to the known resonance wavelengths, these data have been corrected by −2.5 pm. The intensities of all three laser beams were converted from their total beam intensities (as measured) to average beam intensities, although the model intensity that best describes the experimental data is a factor of five smaller than the actual laser intensity in the ionization volume (see below). The laser pulses were fixed in the model to arrive simultaneously, each as a Gaussian distribution with FWHM of 20 ns. The modeled pulses were broadened by summing with a second Gaussian distribution of 14 ns (FWHM) to approximate

[7]The experiment was performed with the third laser tuned to 722.344 nm, and the cross section at this wavelength is about 62.5 % of the peak cross section at 722.200 nm. The peak cross section used in the model for this resonance was reduced accordingly.

the average distribution of the pulse amplitude over many laser pulses[8]. For the narrow bandwidth experiment the empirical value of the ^{238}U off-resonance ion signal is 2.6 ± 0.2 % of the maximum on-resonance ion signal, while for the broad bandwidth experiment a value of 1 % was used for the off-resonance correction as determined by experiment.

Figure 0.5 shows a comparison of data from these experiments with the corresponding model predictions for the variation in the $^{235}\mathrm{U}/^{238}\mathrm{U}$ ratio relative to the certified ratio as a function of the wavelength of the first of three excitation lasers for two different laser bandwidths (1 and 5 pm). The slopes of the model predictions near the center of the plot (around 415.51 nm) demonstrate the sensitivity of the measured isotope ratio to variations in the mean laser wavelength. Uncertainties in the measured isotope ratio are not displayed, but are less than 1% of the relative values, smaller than the symbols in the figure. The extremely steep slope (note the logarithmic scale) for the narrow laser bandwidth, indicates that even small variations in the laser wavelength produce large fractionations in the measured isotope ratio. For the broad laser bandwidth, ionization for both isotopes is nearly saturated at wavelengths near the isosbestic point, and the measured isotope ratio shows much less sensitivity to laser wavelength variation. It is worth noting that the enhancement of the ionization of ^{235}U over ^{238}U near the isosbestic point is consistent between both the model predictions and experimental measurements for broad bandwidth. This suggests that while the broadband approach to measuring isotope ratios via RIMS may not be free of fractionation associated with the ionization process, the magnitude of the fractionation can be minimized, and the model appears to capture the most significant factors governing the wavelength dependence of the isotope ratio.

[8]This is a linear approximation to what is certainly a non-linear dependence on the relative laser pulse timing, and may contribute to differences between the experimental beam intensity and values representing the best-fit for the model.

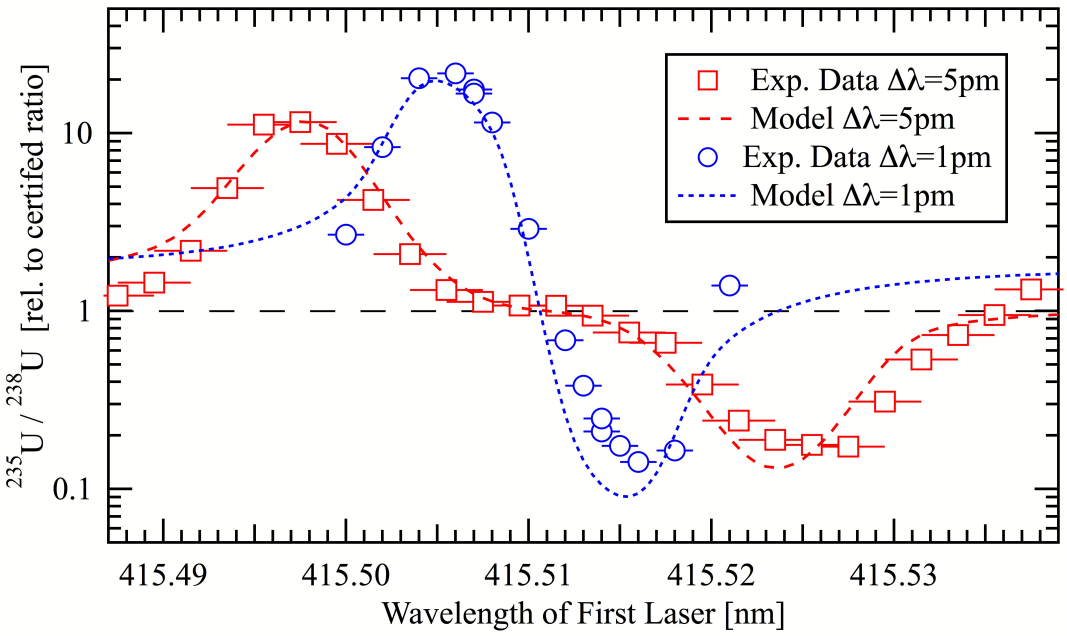

Figure 0.5: The measured and predicted $^{235}U/^{238}U$ ratio, relative to the respective certified ratio of the standards, as a function of the wavelength of the first of three excitation lasers used in RIMS analyses of U isotopes for two bandwidths, $\Delta\lambda$ = 1 and 5 pm. Deviation from the dashed line at $^{235}U/^{238}U = 1$ represents fractionation of the measured isotope ratio relative to the known value of the standards.

MODEL RESULTS

Two additional experiments were conducted using CRM U500 to investigate the sensitivity of the measured isotope ratio to laser irradiance as a function of first laser wavelength when the first laser has a broad spectral bandwidth. The experimental conditions were very similar to those described above, but with the average energy of the first laser set to 150 and 530 μJ per pulse, while the second and third lasers had average energies of 960, and 610 μJ per pulse, respectively. The measured pulse-to-pulse fluctuation of the mean wavelength of the first laser was also somewhat larger, ~ 6.5 pm for these experiments. Model calculations were identical to those discussed above apart from the mean wavelength fluctuation and the laser irradiances, which were scaled linearly with the differences in total energy. A comparison of results for the two broad bandwidth experiments and model calculations for two average laser irradiances is shown in Figure 0.6. The uncertainties in mean wavelength for the measured data have been omitted for clarity, but are similar to those from the broad bandwidth data in Fig. 0.5.

The most notable differences between the two experiments are the amplitude of the maximum and minimum isotope ratio that are less extreme for the 530 μJ experiment, and the slope near the isosbestic point that is also decreased at higher irradiance. These differences are mainly due to two factors, an increase in the non-resonant background measured in the 235 and 238 mass peaks, and power broadening. The non-resonant background signal at both masses is approximately doubled when the irradiance of the first laser is increased from 150 μJ to 530 μJ. This is the main source of the significant decrease in the maximum and minimum deviation of the measured isotope ratio, where the non-resonant background ion signal is comparable in magnitude to the ionization probability of the off-resonance isotope. For example, near the peak at 415.500 nm over 95 % of the ^{235}U is ionized, but less than 1% of the available ^{238}U is resonantly ionized, while the non-resonant background at both masses is around 1 % and 2 % for the 150 and 530 μJ experiments,

respectively. Thus, the non-resonant signal can have a factor of 2 effect on the measured isotope ratio at wavelengths where only one isotope is being resonantly ionized with significant probability. In regions where both isotopes are being ionized with significant probability (*i.e.*, near the isosbestic point), however, the non-resonant ion signal contributes only 1 or 2 % to the measured signal at the masses of interest. Power broadening, the apparent broadening of an atomic resonance lineshape with increasing irradiance, is an additional effect (besides increasing bandwidth) decreasing the sensitivity of the measured isotope ratio near the isosbestic point to variations in mean wavelength from pulse to pulse [44]. For these experiments, the slope near the isosbestic point of the data for 530 μJ decreases by about 25 % relative to the data at 150 μJ. For comparison, the results described in Fig.0.5 show that the slope in that region decreases by a factor of ~50 by increasing bandwidth from 1 pm to 5 pm. Although power broadening may decrease the sensitivity of the measured isotope ratio to fluctuations in the mean wavelength of the lasers, the power of each laser must be optimized to consider both the saturation of a given transition, as well as its contribution to non-resonant ionization. The model predictions for these experiments appear to account for the main differences between the results of the experiments performed at different laser irradiances, despite the difficulties of translating actual laser irradiances into appropriate point model averages, as discussed below.

Discussion

Our experiments involve a three-dimensional distribution of photon flux interacting with the cloud of desorbed neutral species, also distributed in three dimensions. The model neglects the spatial distribution of photon flux and the time-evolving spatial distribution of neutral atoms in the ionization volume, both of which would produce nonlinear effects on the total ionization probabil-

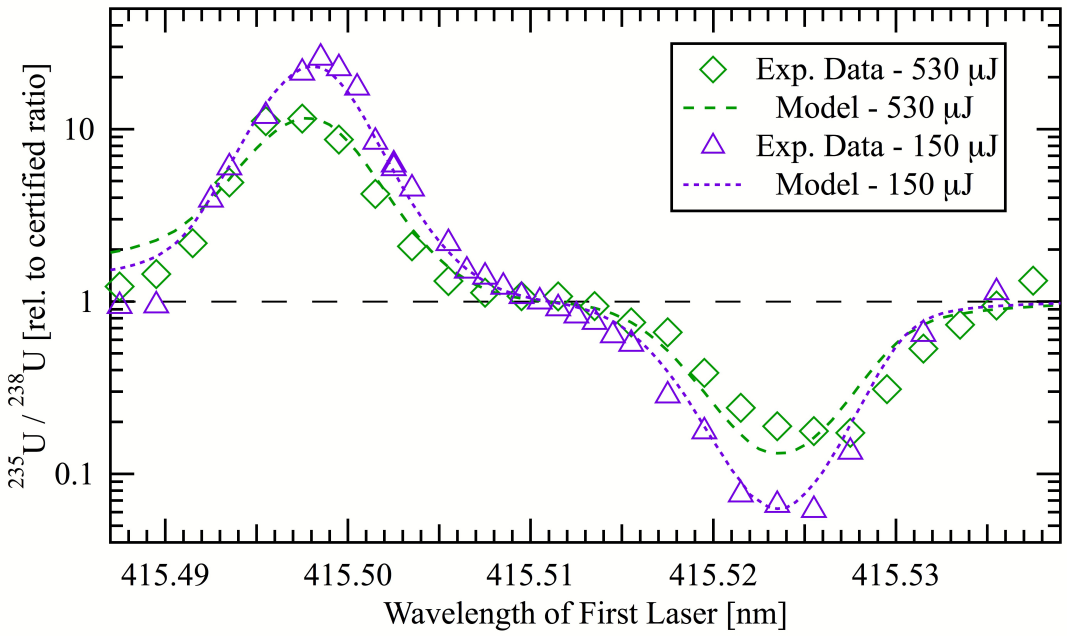

Figure 0.6: The measured and predicted $^{235}U/^{238}U$ ratio, relative to the certified ratio, as a function of the wavelength of the first of three excitation lasers used in RIMS analysis of U isotopes for two values of laser irradiance, 150 and 530 μJ. The dashed line at $^{235}U/^{238}U = 1$ represents the certified isotope ratio value for this standard, CRM U500.

ity. Within this limitation, the model suggests that laser intensity is a dominant factor affecting the variation of the measured isotope ratios from their known value. Significantly, the modeled laser intensity in the ionization volume that best describes the data is a factor of 5 or 6 smaller than the measured laser intensity in these experiments. Spatially saturating the ionization of atoms near the high-intensity center of the laser beams is not accounted for, reducing the *apparent* laser intensity in the ionization volume. Photons found in any volume where the ionization has been saturated have no additional atoms to ionize, and do not contribute to the ionization probability. In addition, the method used for distributing the amplitude of the laser pulse as an average intensity over many laser pulses likely over-estimates the overlap of the time-dependent laser amplitudes relative to each other. Taken together, these effects reduce the effective intensity of the laser beams in the ionization volume. This difference highlights the need for a better representation of the spatial distribution of photon intensity, the atom density, and their superposition in the ionization volume.

Our approximation that the mean wavelength variation and laser pulse time distribution can be averaged over many laser pulses clearly neglects the nonlinear effects arising from the combination of these two parameters that, given the variations observed experimentally, must have an effect on the experimentally measured isotope ratios. While the discrete averaging of these parameters leads to an overall understanding of the variation in the ionization probability as a function of wavelength, the comparison with experimental data is likely to fall short when the stochastic effects of laser performance are neglected. The model has been constructed to allow the stochastic variation of a number of laser parameters, but, thus far, only a limited number of cases have been examined. In general, stochastic sampling will tend to produce more smoothly varying results as a function of laser wavelength than might exist in the absence of significant statistical variation in parameters. For example, the effect of stochastic variation of laser timing on the model predictions will

be strongly dependent on the intensity of the laser beams, as the superposition of pulses will be dependent on the pulse amplitude. This is a shortcoming of our choice not to allow the stochastic variation of laser timing in our single point model of laser beam intensity, as the approximation that results from this choice does not accurately relate the modeled beam intensity to the actual intensity. The stochastic variation of laser pointing stability (the movement of the beam center from pulse-to-pulse) has not been considered, but significant variations in beam position relative to the beam width should produce an effect very similar to the variation in laser pulse timing.

Conclusions

We have demonstrated that spectroscopic information, combined with empirical corrections, can be used to predict the relative ionization probabilities of uranium isotopes for a variety of laser parameters and, therefore, provides a viable approach to design and evaluate robust RIMS methods for specific elements and isotopes of interest. The calculations discussed here have not only been demonstrated as a basis for understanding the most significant factors affecting laser-induced isotope fractionation, but also aid in identification of factors of laser design and stability that should be the focus of technological improvements for the purpose of applying RIMS to the direct measurement of the relative isotopic abundances of uranium without chemical manipulation of samples. Specifically, this method can be used to identify the optimal laser irradiances for minimizing laser induced bias given the atomic cross sections, laser bandwidths, and the dependence of non-resonant background on laser irradiance.

The model predictions for the decreased sensitivity of the measured isotope ratio to variations in mean wavelength are consistent with recent measurements on the CHARISMA instrument using broad bandwidth lasers with improved wavelength and timing stability that demonstrated 0.3%

reproducibility and total measurement biases of 2-5% for the $^{235}U/^{238}U$ ratio [12]. The improved reproducibility of these measurements enabled, for the first time, the observation and study of instrument biases on CHARISMA that could not be explained by laser induced fractionation (both resonant ions and non-resonant ions had almost identical biases). Subsequent improvements to the instrument tuning and operation have facilitated the quantification of Pu isotope ratios to accuracy and precision of 1% or better [14], where laser induced biases and instrument effects are now on the same order of significance for accurately quantifying isotope ratios by RIMS.

There are two main improvements that will be pursued to improve the model and produce a more accurate characterization of the RIMS ionization process: *(i)* more realistic spatial distributions of laser irradiance and neutral atom densities in the ionization volume to provide a weighted average of the relative ionization probability, and *(ii)* the stochastic variation of irradiance as a function of time, position, and wavelength using empirical probability distribution functions. The nonlinear effects of averaging laser wavelength and pulse timing are important to understanding variations in measured isotope ratios, and must be considered in future work to better define the actual values of laser parameters during the experiments. Realistic spatial distributions will enable the model to reproduce the compounding effects of variations in laser parameters, and improve the quality of the calculated values of the cross sections. Finally, improved characterization of broad laser spectral distributions should be pursued, to provide a higher fidelity description of broad bandwidth, multi-mode laser spectral distributions.

Future efforts will also expand the rate equation model to incorporate the relative ionization probability of other elements of interest such as Pu. This requires detailed spectroscopic information for resonance ionization schemes for each element. Some of the necessary data are available in the literature [45], but most of the spectroscopic information is incomplete. In addition, there

are several additional parameters that must be measured to obtain a complete understanding of the relative ionization probability. Specifically, the cross sections for photo-ionization of the excited atoms by all allowed single-photon transitions are required, as is the influence of non-zero angular momentum (for odd isotopes) on the cross sections. These parameters can be obtained by measuring the rates of change of the ionization probability as a function of the appropriate laser intensities as in Fig. 0.4. Rare and/or highly radioactive isotopes that are difficult to work with experimentally can also be studied using these computational models, if sufficient atomic spectroscopic information is available.

Acknowledgements

This work performed under the auspices of the U.S. Department of Energy by Lawrence Livermore National Laboratory under Contract DE-AC52-07NA27344. The CHARISMA facility at Argonne National Laboratory is supported by the U.S. Department of Energy, Office of Science, Materials Sciences and Engineering Division. The authors are grateful for support from the U.S. Department of Homeland Security's National Technical Nuclear Forensics Center, including funding for the experimental effort of B.H.I., K.B.K., M.R.S and D.G.W. This work was supported, in part, by the Defense Threat Reduction Agency (DTRA) through Award No. HDTRA 135636-M. Manuscript preparation at LLNL was funded by the Laboratory Directed Research and Development Program at LLNL under project tracking code 14-ERD-082. LLNL-JRNL-648449.

References

References

[1] X. Hou and P. Roos, *Anal. Chim. Acta*, 2008, **608**, 105–139.

[2] Y. Ranebo, P. Hedberg, M. Whitehouse, K. Ingenerid and S. Littmanna, *J. Anal. At. Spectrom*, 2009, **24**, 277–287.

[3] S. Raeder, S. Fies, H. Tomita and K. D. A. Wendt, *4th Int. Conf. on Laser Probing - LAP 2008, AIP Conf. Proceedings*, 2009, **1104**, 96–101.

[4] K. Wendt and N. Trautmann, *Int. J. Mass Spectrom.*, 2005, **242**, 161–168.

[5] N. Erdmann, J.-V. Kratz, N. Trautmann and G. Passler, *Anal. Bioanal. Chem.*, 2009, **395**, 1911–1918.

[6] J. Levine, M. Savina, T. Stephan and M. Pellin, *4th Int. Conf. on Laser Probing - LAP 2008*, 2009, **1104**, 90–95.

[7] M. R. Savina, M. J. Pellin, C. E. Tripa, I. V. Veryovkin, W. F. Calaway and A. M. Davis, *Geochim. Cosmochim. Acta*, 2003, **67**, 3215–3225.

[8] J. G. Barzyk, M. R. Savina, A. M. Davis, R. Gallino, M. J. Pellin, R. S. Lewis, S. Amari and R. N. Clayton, *New Astron. Rev.*, 2006, **50**, 587–590.

[9] G. Nicolussi, M. Pellin, K. Lykke, J. Trevor, D. Mencer and A. Davis, *Surf. Interface Anal.*, 1996, **24**, 363–370.

[10] B. H. Isselhardt, *Quantifying Uranium Isotope Ratios Using Resonance Ionization Mass Spectrometry: The Influence of Laser Parameters on Relative Ionization Probability*, Ph.D. Dissertation, University of California, Berkeley, 2011.

[11] B. H. Isselhardt, M. R. Savina, K. B. Knight, M. J. Pellin, I. D. Hutcheon and S. G. Prussin, *Anal. Chem.*, 2011, **83**, 2469–2475.

[12] B. H. Isselhardt, M. R. Savina, D. G. Willingham, K. B. Knight and I. D. Hutcheon, *Proc. of the INMM*, 2013.

[13] K. Knight, M. Savina, B. Isselhardt, I. Hutcheon, S. Prussin and M. Pellin, *Proc. in Radiochem.*, 2011, **1**, 37–43.

[14] B. Isselhardt, M. Savina, A. Kucher, S. Gates, K. Knight and I. Hutcheon, *J. Radioanal. Nucl. Chem.*, 2015, 1–8.

[15] D. Willingham, M. R. Savina, K. B. Knight, M. J. Pellin and I. D. Hutcheon, *J. Radioanal. Nucl. Chem.*, 2013, 1–6.

[16] N. Shimizu and S. R. Hart, *J. Appl. Phys.*, 1982, **53**, 1303–1311.

[17] M. Payne, S. Allman and J. Parks, *Spectrochim. Acta, Part B*, 1991, **46**, 1439–1457.

[18] M. Payne, L. Deng and N. Thonnard, *Rev. Sci. Instrum.*, 1994, **65**, 2433–2459.

[19] R. Wunderlich, I. Hutcheon, G. Wasserburg and G. Blake, *Appl. Spect. Mat. Sci. 11*, 1992, **1636**, 211.

[20] R. Wunderlich, G. Wasserburg, I. Hutcheon and G. Blake, *Anal. Chem.*, 1993, **65**, 1411–1418.

[21] P. Lambropoulos and A. Lyras, *Phys. Rev. A*, 1989, **40**, 2199–2202.

[22] A. Lyras, B. Zorman and P. Lambropoulos, *Phys. Rev. A*, 1990, **42**, 543–549.

[23] B. W. Shore, *Phys. Rev. A*, 1978, **17**, 1739–1746.

[24] W. Whitten and J. Ramsey, *Appl. Spectrosc.*, 1990, **44**, 1188–1192.

[25] S. Swain, *J. Phys. B: At. Mol. Phys.*, 1982, **15**, 3405.

[26] M. Sankari, P. Kumar and M. Suryanarayana, *Int. J. Mass Spectrom.*, 2006, **254**, 94–100.

[27] J. R. Ackerhalt and B. W. Shore, *Phys. Rev. A*, 1977, **16**, 277–282.

[28] J. R. Ackerhalt, J. H. Eberly and B. W. Shore, *Phys. Rev. A*, 1979, **19**, 248–263.

[29] P. Schumann, K. Wendt and B. Bushaw, *Spectrochim. Acta, Part B*, 2005, **60**, 1402–1411.

[30] W. Childs, O. Poulsen and L. Goodman, *Opt. Lett*, 1979, **4**, 4–1.

[31] D. Suter, *The physics of laser-atom interactions*, Cambridge University Press, 1997.

[32] A. Edmonds, *Angular momentum in quantum mechanics*, Princeton University Press, 1996.

[33] B. W. Shore and M. A. Johnson, *Phys. Rev. A*, 1981, **23**, 1608.

[34] R. Wright, M. Pellin and D. Gruen, *Nucl. Instrum. Methods*, 1981, **182**, 167–178.

[35] A. Coste, R. Avril, P. Blancard, J. Chatelet, D. Lambert, J. Legre, S. Liberman and J. Pinard, *J. Opt. Soc. Am*, 1982, **72**, 103–109.

[36] M. Miyabe, M. Oba and I. Wakaida, *J. Phys. B: At., Mol. Opt. Phys.*, 2000, **33**, 4957–4972.

[37] M. Smyth, L. Green, F. Sopchyshyn and P. Leeson, *J. Phys. B: At., Mol. Opt. Phys.*, 1991, **24**, 4887.

[38] S. L. Ziegler and B. A. Bushaw, *Anal. Chem.*, 2008, **80**, 6029–6033.

[39] E. Miron, R. David, G. Erez, S. Lavi and L. A. Levin, *J. Opt. Soc. Am.*, 1979, **69**, 256–264.

[40] Z. Ma, R. Thompson, K. Lykke, M. Pellin and A. Davis, *Rev. Sci. Instrum.*, 1995, **66**, 3168.

[41] M. G. Hurst, G. S. Payne, *Principles and Applications of Resonance Ionisation Spectroscopy*, A. Hilger, 1988.

[42] New Brunswick Laboratory, *Certificate of Analysis CRM 112-A Uranium (normal) Metal Assay and Isotopic Standard*, US Department of Energy, http://science.energy.gov/nbl, 2010.

[43] New Brunswick Laboratory, *Certificate of Analysis CRM U500 Uranium Isotopic Standard*, US Department of Energy, http://science.energy.gov/nbl, 2008.

[44] J. Levine, M. Savina, T. Stephan, N. Dauphas, A. Davis, K. Knight and M. Pellin, *Int. J. Mass Spectrom.*, 2009, **288**, 36–43.

[45] J. E. Sansonetti, W. C. Martin and S. Young, *J. Phys. Chem. Ref. Data*, 2005, **34**, 1559–2260.